

Full reference point cloud quality assessment using support vector regression

Ryosuke Watanabe^{a,b,*}, Shashank N. Sridhara^b, Haoran Hong^b, Eduardo Pavez^b, Keisuke Nonaka^a, Tatsuya Kobayashi^a, Antonio Ortega^b

^aKDDI Research, Inc., 2-1-15 Ohara, Fujimino, 356-8502, Saitama, Japan

^bUniversity of Southern California, 3650 McClintock Ave, Los Angeles, 90089, California, United States

Abstract

Point clouds are a general format for representing realistic 3D objects in diverse 3D applications. Since point clouds have large data sizes, developing efficient point cloud compression methods is crucial. However, excessive compression leads to various distortions, which deteriorates the point cloud quality perceived by end users. Thus, establishing reliable point cloud quality assessment (PCQA) methods is essential as a benchmark to develop efficient compression methods. This paper presents an accurate full-reference point cloud quality assessment (FR-PCQA) method called full-reference quality assessment using support vector regression (FRSVR) for various types of degradations such as compression distortion, Gaussian noise, and down-sampling. The proposed method demonstrates accurate PCQA by integrating five FR-based metrics covering various types of errors (e.g., considering geometric distortion, color distortion, and point count) using support vector regression (SVR). Moreover, the proposed method achieves a superior trade-off between accuracy and calculation speed because it includes only the calculation of these five simple metrics and SVR, which can perform fast prediction. Experimental results with three types of open datasets show that the proposed method is more accurate than conventional FR-PCQA methods. In addition, the proposed method is faster than state-of-the-art methods that utilize complicated features such as curvature and multi-scale features. Thus, the proposed method provides excellent performance in terms of the accuracy of PCQA and processing speed. Our method is available from <https://github.com/STAC-USC/FRSVR-PCQA>.

Keywords: point cloud quality assessment, full-reference, support vector regression, graph signal processing

1. Introduction

Point clouds are utilized to represent realistic 3D objects in a variety of 3D applications such as telepresence [1], autonomous driving [2], monitoring [3], and holographic display [4]. These applications may introduce distortions during the scanning, compression, transmission, storage, and rendering processes. These distortions may degrade the perceptual quality of point clouds.

In recent years, efficient point cloud compression and quality enhancement have been studied to mitigate the impact of distortions. For instance, the MPEG committee is developing two standards for point cloud compression: geometry-based point cloud compression (G-PCC) and video-based point cloud compression (V-PCC) [5]. Moreover, compression methods based on deep learning have emerged as alternative approaches to improve coding efficiency [6, 7]. Furthermore, many methods aiming at improving the quality of point clouds have been proposed to alleviate the impact of distortions (e.g., point cloud denoising [8, 9], upsampling [10, 11], and inpainting [12, 13]). Under the circumstances, point cloud quality assessment (PCQA) methods are important benchmarks in these studies. Hence, establishing reliable PCQA methods helps develop high-performance compression and quality enhancement.

In contrast to quality assessment methods for 2-D images or videos [14, 15, 16], where only color information is utilized, perceptual quality of 3D content is significantly influenced by *both* geometry and color distortion and their interactions. Thus, PCQA methods should consider both types of distortions. Consequently, quality assessment methods developed for 2D images or videos cannot be directly extended to PCQA. Methods for PCQA are categorized into full-reference PCQA (FR-PCQA), reduced-reference PCQA (RR-PCQA), and no-reference PCQA (NR-PCQA) approaches. Unlike RR-PCQA and NR-PCQA metrics, FR-PCQA methods provide stable assessments because they compare a distorted point cloud with the reference point cloud. Due to this stability, some FR-PCQA metrics [17, 18] have been employed as criteria for establishing effective compression methods in the MPEG standardization [5]. While these methods [17, 18] focus on point-wise errors, other methods that consider (i) more complex features (e.g., structural similarity [19, 20, 21]), (ii) graph similarity [22, 23], or (iii) learning-based techniques [24, 25] have been proposed to improve the PCQA accuracy.

The challenges with a conventional PCQA method are assessment accuracy and computation speed. Regarding PCQA accuracy, although (i) more complex features and (ii) graph similarity can enhance the accuracy of point-wise errors, the PCQA accuracy is still limited. This is because the simple combination such as a linear combination [20, 21] or multiplication [22, 23] of multiple metrics has been introduced. In con-

*Corresponding author at KDDI Research, Inc. (2-1-15 Ohara, Fujimino, Saitama, 356-8502, Japan), E-mail address: ru-watanabe@kddi.com (R. Watanabe).

trast, incorporating (iii) learning-based techniques significantly improves accuracy. However, these advancements suffer from slow assessment speed. In particular, computational complexity is a problem when we consider a large point cloud or point cloud video (dynamic point clouds).

This paper introduces a novel FR-PCQA method, full-reference quality assessment using support vector regression (FRSVR)¹. Since the proposed method can integrate multiple simple metrics effectively based on support vector regression (SVR), it achieves a superior trade-off between PCQA accuracy and computation speed. Our proposed FRSVR obtained the first place in the FR broad-range quality estimation results track in the ICIP 2023 point cloud visual quality assessment grand challenge (ICIP 2023 PCVQA Grand Challenge) [26].

1.1. Contributions of this paper

Our main contributions are:

1. We propose an accurate FR-PCQA by integrating five types of FR metrics using SVR. Since the five metrics cover various errors (e.g., geometry, color, point count, point-to-point, and region-to-region errors), we achieve excellent objective quality assessment accuracy. In addition, we achieve a favorable computation speed because the five metrics share several steps, such as neighborhood search and graph construction.
2. We comprehensively evaluated accuracy and computation time on three public datasets and verified the effectiveness of our method for various data and distortion types, not only the compression distortions evaluated in the ICIP 2023 PCVQA Grand Challenge.
3. For further improvement of the accuracy of the proposed method, we experimented with the combination with scores other than the five types of scores mentioned above. We observed that the accuracy exceeded our ICIP 2023 PCVQA Grand Challenge results. These results are introduced in Section 5 as extra experiments. The additional scores are obtained from PCQM [21], which is a state-of-the-art PCQA method that utilizes a linear combination of various types of FR-PCQA scores.

The proposed methodology described in the first contribution was designed for the ICIP 2023 PCVQA Grand Challenge [27], which aims to assess compression distortions. The second and third contributions are new.

1.2. Structure of this paper

The remainder of this paper is organized as follows: Section 2 provides a comprehensive review of related work in PCQA. Section 3 introduces the details of the proposed method. Section 4 shows the experimental results that verify the effectiveness of the proposed method. Based on the experimental results, Section 5 shows the limitations of the proposed method and strategies for further improvement. Finally, we conclude the paper in Section 6.

¹Source code of the proposed method is available at <https://github.com/STAC-USC/FRSVR-PCQA>.

2. Related work

PCQA methods are categorized into the following three classes according to whether reference point clouds are required: (1) NR-PCQA, (2) RR-PCQA, and (3) FR-PCQA.

2.1. No-reference PCQA (NR-PCQA) methods

NR-PCQA methods can be applied when reference point clouds are not available. Learning-based approaches are mainstream for NR-PCQA. Some methods perform 3D-to-2D projection and then use NR image quality assessment based on convolutional neural networks [28, 29, 30]. As an alternative that does not require projections, methods using 3D deep neural networks [31, 32, 33] and graph neural networks [34, 35] have been proposed. While neural network-based approaches achieve accurate quality assessment, the processing time increases due to 3D-to-2D projection or inference with deep neural networks. Methods using SVR have been proposed [36, 37] as alternatives to neural network techniques, demonstrating a favorable trade-off between computation speed and accuracy. However, the stability and robustness of NR quality assessment can be low because the results generally depend strongly on the training data’s characteristics.

2.2. Reduced-reference PCQA (RR-PCQA) methods

RR-PCQA approach utilizes partial information in a reference point cloud for PCQA. Viola and Cesar [38] propose an RR-PCQA method using a small set of statistical features from the reference point cloud. Liu et al. [39] utilize the attribute and geometry quantization steps of point cloud compression methods to infer the point cloud quality. Zhou et al. [40] introduce an image-based RR-PCQA method via saliency projection. The content-oriented similarity and statistical correlation calculated from saliency maps are utilized to estimate the perceptual quality of a point cloud. Since the accuracy of RR-PCQA depends on the extracted features, it can decrease if the features are not robust or fail to capture critical point cloud information.

2.3. Full-reference PCQA (FR-PCQA) methods

FR-PCQA methods, which are the focus of this paper, necessitate a high-quality (noise-free) reference point cloud for each distorted point cloud. They can be classified into four groups based on (1) projection, (2) 3D geometry, (3) geometry and color, and (4) learning. Our method makes use of geometry and color metrics and combines them using a simple learning strategy.

2.3.1. Projection-based methods

Projection-based methods utilize conventional 2D image quality assessment techniques after projecting a 3D point cloud onto a 2D plane. A recent framework [41] predicts point cloud quality by applying 2D image quality assessment metrics (e.g., SSIM [15], MS-SSIM [16], VIFP [42]) to multiple projected views. Liu et al. [43] provide an attention-guided PCQA inspired by the information content weighted-structural similarity

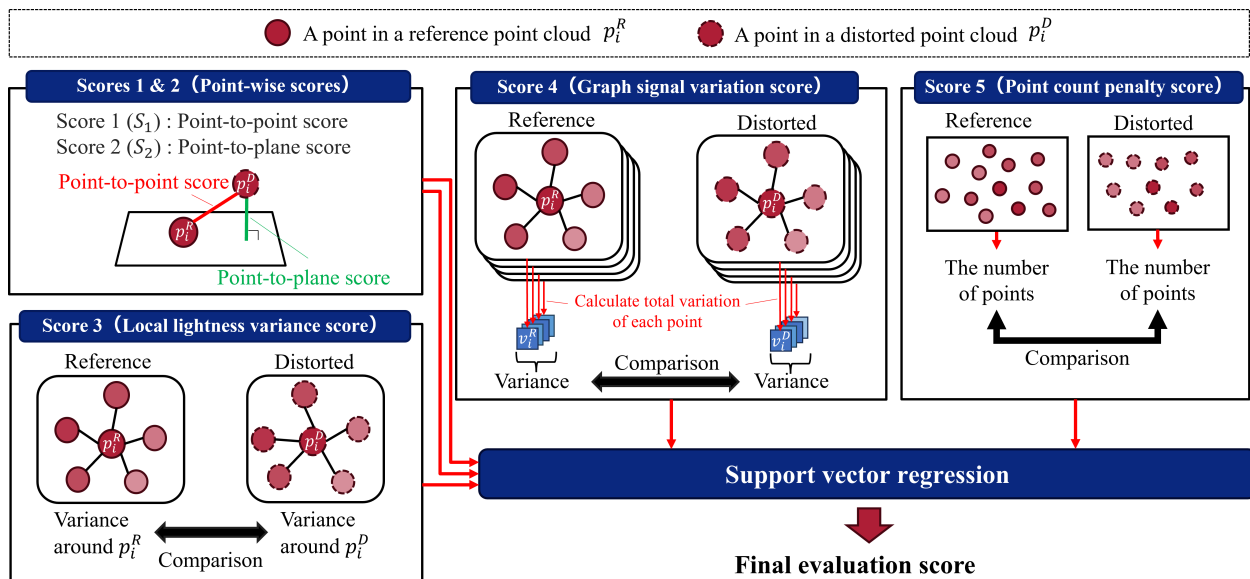


Figure 1: The calculation flow of the proposed method. The five FR-PCQA scores are utilized to predict the final evaluation score by SVR.

measure [44]. To enhance the perception of geometric distortion, curvature projection is utilized to extract geometric statistical features [45]. Since these approaches result in the loss of 3D information during the projection from 3D to 2D, the assessment accuracy may be occasionally degraded. Besides, the choice of projection process and the number of viewpoints can negatively impact the accuracy of the final prediction.

2.3.2. 3D geometry-based methods

3D geometry-based methods measure geometric distortion in point clouds. Point-to-point error [17] and point-to-plane error [18] are popular metrics for assessing geometric distortion. The former measures the distance between each point of the distorted point cloud and its corresponding nearest neighbor point in the reference point cloud. The latter refers to the projection error in the normal vector direction of the nearest point in the reference point cloud. Also, Alexiou et al. [46] proposed an FR-PCQA method using angular similarity of tangent planes among corresponding points. These methods are constrained because they only consider geometry.

2.3.3. 3D geometry and color-based methods

Some FR-PCQA methods consider both geometric and color distortion. Geometric distortion can indirectly affect color distortion because the positional correspondence between the distorted and reference point clouds is required to compute color distortion. Regarding color distortion, the Peak Signal-to-Noise Ratio (PSNR) is a benchmark in MPEG standardization [17]. As an alternative, PointSSIM [19], an extension of SSIM [15] for point clouds, compares statistical information of small regions, such as color variance. PCQA accuracy is limited since these methods compare only one feature derived from color components (e.g., color itself or color variance around a point). To improve accuracy, PCQM [21] is calculated using

a weighted linear combination of geometric and color distortion metrics. Moreover, a graph-based FR-PCQA method [22] has been proposed to measure distortion using a graph structure constructed from point clouds. Computation cost is high since these methods utilize complex features, such as curvature, to improve accuracy. Furthermore, methods that perform multi-scale comparisons have also been proposed to improve the accuracy [20, 23]. However, these methods significantly increase calculation time.

2.3.4. Learning-based methods

In recent years, learning-based approaches have been introduced to obtain better accuracy. An end-to-end deep-learning framework [24] is proposed for accurate FR-PCQA, considering both geometry and color information. Another approach [25] utilizes PCA-based features to predict the evaluation score. While these methods demonstrate high accuracy by combining geometry and color information, they suffer from high computation costs [26].

3. Proposed method

3.1. Overview

This section introduces the proposed FR-PCQA method, FRSVR (see Fig. 1). In the training process, an SVR model [47] is trained using five types of FR scores ($S_1 \sim S_5$), namely: (1) point-to-point score S_1 , (2) point-to-plane score S_2 , (3) local lightness variance score S_3 , (4) graph signal variation score S_4 , and (5) point count penalty score S_5 . The S_1 and S_2 scores represent geometric distortion. In contrast, the S_3 and S_4 scores quantify local and global lightness differences between distorted and reference point clouds. Since a KNN graph constructed by coordinate values is utilized to calculate the S_3 and S_4 scores, they are affected by both lightness and geometric distortions. S_5 captures the difference in the number of points. All

scores are such that $S_i \in [0, 1]$, with larger values indicating better quality. Then, SVR is used to integrate the scores related to geometry, lightness, and the number of points.

3.2. Preliminaries

Distorted and reference point clouds are represented as $P_D = \{p_i^D\}$, $i = 1, \dots, |P_D|$ and $P_R = \{p_j^R\}$, $j = 1, \dots, |P_R|$, respectively, where $|P_D|$ and $|P_R|$ denote the number of points. Point p_i^D has 3D coordinates $\mathbf{g}_i^D \in \mathbb{R}^3$ and associated RGB color $\mathbf{c}_i^D \in \mathbb{R}^3$ (Likewise, p_j^R has \mathbf{g}_j^R and \mathbf{c}_j^R). The proposed method uses the lightness (L) term of each point $p_i^D \in \mathbb{R}$ that is calculated by color conversion from RGB color space (\mathbf{c}_i^D) to LAB color space [48] before calculating the scores, as is done in the conventional PCQA method [21].

In the proposed method, we construct an undirected graph, $\mathcal{G} = (\mathcal{V}, \mathcal{E})$, from the point cloud to calculate the metrics. We use the Euclidean distance; each point is connected to its K nearest neighbors (KNN). \mathcal{V} and \mathcal{E} indicate the sets of nodes and edges on the graph, respectively. The points in the set $\mathcal{N}(p_j)$ are the neighbors of p_j .

3.3. Point-to-point score

The point-to-point error [17] is the sum of geometric distances between every point in one point cloud and the corresponding closest point in the other. The point-to-point error from the reference point cloud P_R to the distorted point cloud P_D is calculated as

$$E_{p2point}^R = \frac{1}{|P_R|} \sum_{\forall p_i^R \in P_R} \|\mathbf{g}_i^R - \bar{\mathbf{g}}_i^D\|_2^2, \quad (1)$$

where $\bar{\mathbf{g}}_i^D \in \mathbb{R}^3$ are the coordinates of the nearest neighbor for the point p_i^R in the distorted point cloud P_D . Likewise, the point-to-point error from the distorted point cloud P_D to the reference point cloud P_R is calculated as

$$E_{p2point}^D = \frac{1}{|P_D|} \sum_{\forall p_j^D \in P_D} \|\mathbf{g}_j^D - \bar{\mathbf{g}}_j^R\|_2^2. \quad (2)$$

Here, $\bar{\mathbf{g}}_j^R \in \mathbb{R}^3$ are the coordinates of the nearest neighbor of a point p_j^D in the reference point cloud P_R . Next, the point-to-point error $E_{p2point}$ is given as

$$E_{p2point} = \frac{E_{p2point}^R + E_{p2point}^D}{2}. \quad (3)$$

Finally, the score $S_1 \in [0, 1]$ is given by

$$S_1 = \frac{1}{1 + E_{p2point}}. \quad (4)$$

3.4. Point-to-plane score

To calculate the point-to-plane error [18], we projected the error vector $\mathbf{g}_j^D - \bar{\mathbf{g}}_j^R$ introduced in (2) along the normal vector direction of a point. Since the point-to-plane error represents the distance between a point and the surface of a point cloud, it

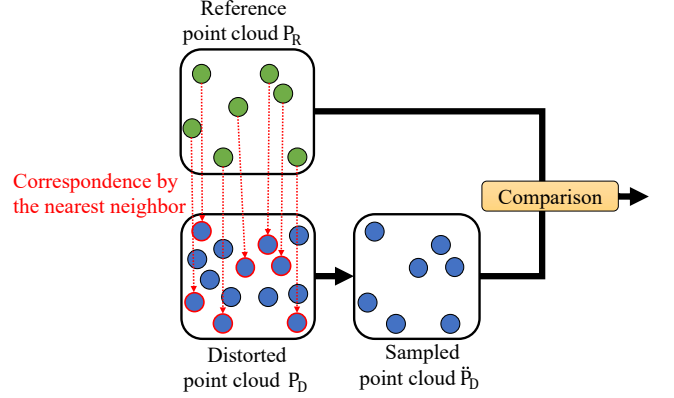


Figure 2: The sampling process to obtain a sampled point cloud \hat{P}_D .

sometimes provides a better PCQA, i.e., closer to human perception than that obtained from point-to-point error. In contrast, if the estimation accuracy of normal vectors is not good, the reliability of the point-to-plane error may be low compared with the point-to-point error. Therefore, our proposed method uses both the point-to-point and point-to-plane errors.

The point-to-plane error from the distorted point cloud P_D to the reference point cloud P_R is given by

$$E_{p2plane}^D = \frac{1}{|P_D|} \sum_{\forall p_j^D \in P_D} ((\mathbf{g}_j^D - \bar{\mathbf{g}}_j^R) \cdot \mathbf{n}_j^R)^2, \quad (5)$$

where \mathbf{n}_j^R is the normal vector corresponding to $\bar{\mathbf{g}}_j^R$. $\mathbf{a} \cdot \mathbf{b}$ denotes the inner product between two vectors, \mathbf{a} and \mathbf{b} . The normal vectors are calculated by a conventional normal estimation method [49]. After that, the point-to-plane score S_2 is calculated by

$$S_2 = \frac{1}{1 + E_{p2plane}^D}. \quad (6)$$

Note that (6) only computes an error from the distorted to the reference point cloud, while in (3), errors in both directions are considered (distorted to reference and vice-versa). This reduces the processing time by a factor of two, while, experimentally, there was almost no difference in PCQA accuracy between the symmetric and asymmetric metrics.

3.5. Local lightness variance score

Unlike S_1 and S_2 , and similar to PointSSIM [19], the local lightness variance score S_3 addresses the distortion of lightness signals in specific regions. Before calculating S_3 , a distorted point cloud P_D is sampled into the sampled distorted point cloud $\hat{P}_D = \{\hat{p}_i^D\}$ as a pre-processing step to reduce computational complexity. Figure 2 shows this sampling process. \hat{p}_i^D is the nearest point from the query point p_i^R . The degradation on PCQA accuracy is pretty small by adapting this sampling strategy. We discuss the impact of this sampling strategy in Section 4.6.

After the sampling, the score S_3 is calculated using P_R and \hat{P}_D as follows:

$$S_3 = \frac{1}{1 + E_{bvar}}, \quad (7)$$

$$E_{bvar} = \frac{1}{|\mathbb{P}_R|} \sum_{\forall p_i^R \in \mathbb{P}_R} (\sigma_i^R - \check{\sigma}_i^D)^2, \quad (8)$$

where,

$$\sigma_i^R = \sqrt{\frac{1}{K} \sum_{\forall p_k^R \in \mathcal{N}(p_i^R)} (l_k^R - \mu_i^R)^2}, \quad (9)$$

$$\check{\sigma}_i^D = \sqrt{\frac{1}{K} \sum_{\forall \check{p}_k^D \in \mathcal{N}(\check{p}_i^D)} (\check{l}_k^D - \check{\mu}_i^D)^2}. \quad (10)$$

σ_i^R and $\check{\sigma}_i^D$ are standard deviations of the respective lightness l_k^R and \check{l}_k^D . Besides, μ_i^R and $\check{\mu}_i^D$ are means of the K nearest neighbors from point p_i^R and \check{p}_i^D , respectively.

3.6. Graph signal variation score

The score S_4 is based on the difference of graph signal variations, which quantify the smoothness of signals on a graph [50]. As with S_3 , we use the sampled $\check{\mathbb{P}}_D = \{\check{p}_i^D\}$ to calculate the score. After that, we compute the total variations of each point in \mathbb{P}_R and $\check{\mathbb{P}}_D$, to form $\mathbf{v}^R = \{v_i^R\}$ and $\mathbf{v}^D = \{v_i^D\}$, with:

$$v_i^R = \sum_{p_k^R \in \mathcal{N}(p_i^R)} |l_i^R - l_k^R|, \quad (11)$$

$$v_i^D = \sum_{\check{p}_k^D \in \mathcal{N}(\check{p}_i^D)} |\check{l}_i^D - \check{l}_k^D|. \quad (12)$$

S_4 is calculated by the difference of the standard deviations of \mathbf{v}^R and \mathbf{v}^D by

$$S_4 = \frac{1}{1 + E_{gvar}}, \quad (13)$$

where

$$E_{gvar} = \frac{|\text{Std}(\mathbf{v}^R) - \text{Std}(\mathbf{v}^D)|}{\text{Std}(\mathbf{v}^R)}. \quad (14)$$

$\text{Std}(\mathbf{a})$ denotes the standard deviation of \mathbf{a} .

Note that the definition of S_4 differs from that in our ICIP challenge paper [27], where we used the sums of (11) and (12). Noise-like errors can produce increases and decreases of the local variation of (11) and (12) for different nodes i . As an alternative, we use the standard deviations of the entries of \mathbf{v}^R and \mathbf{v}^D as shown in (14) instead of (11) and (12). Experimentally, we found that this led to better results.

3.7. Point count penalty score

In general, the number of points has a significant impact on the perceived quality of a point cloud. Specifically, when the number of points in a distorted point cloud $|\mathbb{P}_D|$ is much smaller than that in the reference point cloud $|\mathbb{P}_R|$, the quality of the distorted point cloud \mathbb{P}_D is likely to be low. For example, if a point cloud is compressed with a small bit depth, which leads to a reduction in the number of points in the voxelization process, significant degradation of point cloud quality may be observed, as the point cloud becomes sparse. Thus, we introduce

a point cloud penalty score, S_5 , that evaluates the difference in the number of points as

$$S_5 = \min\left(1, \frac{|\mathbb{P}_D|}{|\mathbb{P}_R|}\right). \quad (15)$$

This penalizes distorted point clouds that have a small number of points as compared with the reference point cloud.

3.8. Support vector regression (SVR)

In the proposed method, SVR is utilized to predict PCQA scores. In the training process, an SVR model is trained with the five scores $S_1 \sim S_5$. The kernel and solver are the Gaussian radial basis function kernel and Sequential Minimal Optimization (SMO) [51], respectively.

4. Experiments

4.1. Experimental conditions

4.1.1. Dataset

We utilized the following three datasets for our experiments: 1) The broad quality assessment of static point clouds in compression scenario dataset (BASICS) [52], 2) The ICIP2020 dataset (ICIP20) [53], and 3) The waterloo point cloud database (WPC) [54]. In the datasets, the mean opinion score (MOS) of the distorted point clouds obtained from a subjective quality assessment is available. 3600, 73, and 60 subjects participated in the subjective evaluation of the BASICS, ICIP20, and WPC datasets, respectively. For all the datasets, the subjects assessed the quality of point clouds with a 2D display that shows point clouds.

- The **BASICS** [52] dataset includes 75 references and 1498 distorted point clouds. The distorted point clouds undergo compression by V-PCC [5], G-PCC [5], or a deep-learning-based compression method [7] at different compression levels.
- The **ICIP20** [53] dataset comprises 6 references and 90 distorted point clouds. Distortions are caused by V-PCC [5] or G-PCC [5].
- The **WPC** [54] dataset consists of 20 references and 740 distorted point clouds. This dataset includes a variety of distorted point clouds, including not only those induced by compression but also by Gaussian noise and down-sampling.

The proposed method was designed for the ICIP 2023 PCVQA Grand Challenge [26], which aims to assess compression distortion introduced in the BASICS dataset [52]. To confirm the effectiveness against compression distortion on another dataset, we experimented with the ICIP20 dataset in this paper. Furthermore, we utilized the WPC dataset to evaluate the applicability to various kinds of noise.

Table 1: The test sets of the ICIP20 [53] and WPC [54] datasets. Two and four kinds of reference data and the corresponding distorted points are utilized for testing in the ICIP20 and WPC datasets, respectively.

Test set	ICIP20 [53]	WPC [54]
Test set 1	[longdress, loot]	[bag, banana, biscuits, cake]
Test set 2	[redandblack, ricardo]	[cauliflower, flowerpot, glasses_case, honeydew_melon]
Test set 3	[sarah, soldier]	[house, litchi, mushroom, pen_container]
Test set 4	N/A	[pineapple, ping-pong_bat, puer_tea, pumpkin]
Test set 5	N/A	[ship, statue, stone, tool_box]

4.1.2. Evaluation Criteria

We employed Pearson’s linear correlation coefficient (PLCC) and Spearman’s rank-order correlation coefficient (SROCC) with respect to the subjective scores to assess the PCQA accuracy of the proposed and the conventional methods. The PLCC and SROCC represent the prediction accuracy and the strength of prediction monotonicity of objective quality assessment metrics, respectively. According to the recommendation for quality assessment [55], a four-parameter logistic regression function [56] was used to calculate the correlation coefficients. In addition, the processing time was measured using a computer equipped with an AMD Ryzen Threadripper 2970WX 24-Core processor, NVIDIA GTX 1080 Ti, and 128GB Random Access Memory.

4.1.3. Training and test scheme

Since the proposed method requires training data, we performed partitioning of each dataset into training and test sets. The BASICS dataset was explicitly divided into training (60%), validation (20%), and test (20%) sets by the authors of the dataset [52]. Thus, we conducted training on the training set and evaluated the performance on the test set. Furthermore, we utilized the validation set for certain validations, such as parameter determination. Both the ICIP20 and WPC datasets were segmented into three and five parts, respectively (See Table 1). Each segment served as an independent test set, while the remaining data were utilized as training data. Following the calculation of PLCC and SROCC for each test set, the average of those was shown as the evaluation result.

4.1.4. Implementation details

In the proposed method, we adopted $K_3 = 20$ and $K_4 = 5$ where K_3 and K_4 indicate the number of neighbors for calculating the S_3 and S_4 scores. The reason is discussed in Section 4.2 along with the experimental results.

As the conventional FR-PCQA for comparison (introduced in Section 4.4), we adopted point-to-point error [17], point-to-plane error [18], angular similarity [46], Y-MSE [17], PointSSIM [19], PCQM [21], GraphSIM [22], and MSGraphSIM [23]. As for PointSSIM [19], though many kinds of implementations are introduced in the original paper [19], we introduced PointSSIM calculated by geometric signals (geom-PointSSIM) and color (color-PointSSIM). The software of conventional FR-PCQA methods, which is provided by the authors, does not utilize GPU acceleration. Thus, for a fair comparison, GPU computing is not utilized for the implementation of the proposed method.

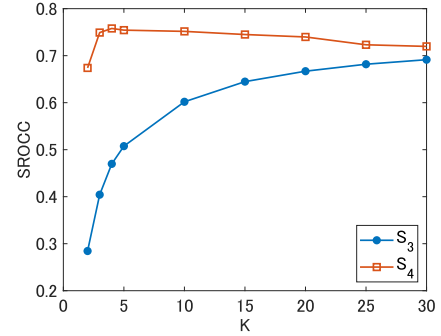


Figure 3: The relationship between the SROCC and the number of neighbors (K) for calculating S_3 and S_4 with the BASICS dataset (validation set).

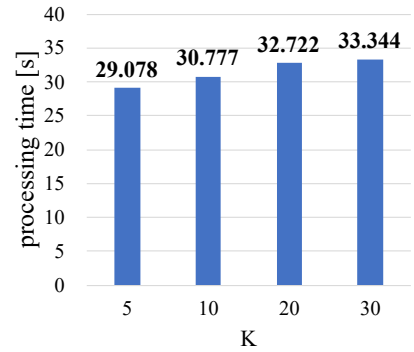


Figure 4: The relationship between the average processing time per point cloud [s] and the number of neighbors (K) with the BASICS dataset (test set).

4.2. Experiment 1: Effects of choices on graph construction parameter

First, we investigated the impact of parameter choices on graph construction. Figure 3 illustrates a relationship between the SROCC and the choices of the parameter K for K nearest neighbors (KNN) with the validation set of the BASICS dataset. In Fig. 3, the line labeled “ S_3 ” indicates the SROCC calculated from only S_3 score without using SVR. As shown in Fig. 3, since the SROCC of the S_4 score saturated at around $K = 5$, we adopted the number of neighbors $K_4 = 5$ for the calculation of S_4 in the following experiments. This is because the values of $\text{Std}(v^R)$ and $\text{Std}(v^D)$ in (14) are strongly influenced not only by noise but also by the color changes in the original (noise-free) signals. The closer the two points are, the more similar their corresponding colors are in an original point cloud. Thus, as K increases, it is the color changes of the original signal, and

Table 2: The correlation coefficient of the test set of the BASICS dataset. The **bold characters** show the best performance.

Score	BASICS (test)	
	PLCC	SROCC
S_1	0.803	0.738
S_2	0.873	0.831
S_3	0.686	0.665
S_4	0.836	0.698
S_5	0.671	0.235
Proposed w/o S_1	0.908	0.858
Proposed w/o S_2	0.909	0.872
Proposed w/o S_3	0.908	0.862
Proposed w/o S_4	0.906	0.877
Proposed w/o S_5	0.910	0.876
Proposed	0.914	0.878

Table 3: The correlation coefficient of the test set of the BASICS dataset with \hat{S}_4 that is introduced in [27]. The **bold characters** show the best performance.

Score	BASICS (test)	
	PLCC	SROCC
\hat{S}_4 [27]	0.818	0.667
S_4	0.836	0.698
Proposed with \hat{S}_4 [27]	0.912	0.875
Proposed with S_4	0.914	0.878

not the noise, that are likely to be reflected in the calculation of standard deviations, $\text{Std}(\mathbf{v}^R)$ and $\text{Std}(\mathbf{v}^D)$. The error E_{gvar} calculated by (14) is influenced by the increase in $\text{Std}(\mathbf{v}^R)$ because the denominator in (14) is $\text{Std}(\mathbf{v}^R)$. As the value of $\text{Std}(\mathbf{v}^R)$ increases due to larger K , the error E_{gvar} may become smaller regardless of noise. Thus, the SROCC slightly decreases as K increases. In contrast, the accuracy of S_3 tends to improve as K increases. Also, Fig. 4 shows the relationship between the overall processing time and the choices of K . The processing time of the proposed method increases as K increases. Considering the balance between the accuracy and processing time, we adopted $K_3 = 20$ for calculating the S_3 score in the following experiments. If accuracy is the primary concern, it may be effective to set larger K .

4.3. Experiment 2: Performance of the proposed method

Table 2 shows the PLCC and SROCC of each metric $S_1 \sim S_5$ and ablation study using the BASICS dataset’s test set. As a single metric, the S_2 score achieved the highest accuracy. Since point cloud information was well integrated using SVR, the combination of five scores dramatically improved the PLCC and SROCC compared with using a single score. Besides, “Proposed w/o S_i ” in Table 2 indicates that S_i score was eliminated to train an SVR model. All the scores were necessary for the proposed method because the accuracy of the proposed method decreased when we removed one of them. In addition, Table 3 compares the S_4 score calculated using (14) and the score \hat{S}_4 we utilized in our ICIP challenge paper [27], as discussed in Section 3.6.

Furthermore, Table 4 shows a breakdown of the calculation time of the proposed method. Before the computation of $S_1 \sim S_4$, color conversion from RGB to L color space and

Table 4: Breakdown of the processing time with the BASICS dataset (test set). These figures are the average processing time across all the point clouds in the dataset.

Part	Time [s]
Color space conversion	0.641
Graph construction	17.090
S_1 calculation	0.014
S_2 calculation	11.897
S_3 calculation	1.919
S_4 calculation	1.159
S_5 calculation	0.001
SVR prediction time	0.001
Total	32.722

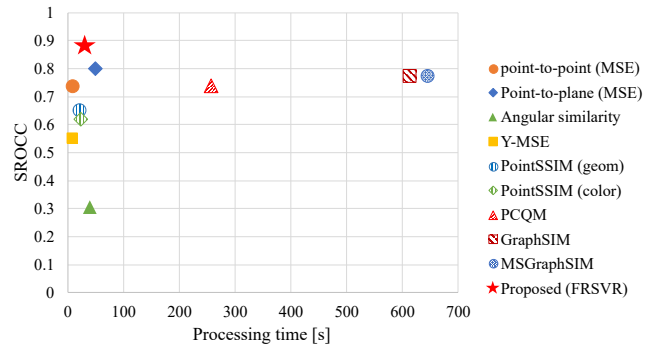


Figure 5: The SROCC and processing time [s] of the proposed method and conventional methods with the BASICS dataset (test set). The upper left of this scatter plot represents a better trade-off between the accuracy and computation speed.

graph construction are carried out. As shown in Table 4, the calculation time for graph construction occupied a large proportion. In addition, since estimating the normal vectors took a long time, the processing time of S_2 became large. Tables 2 and 4 show that eliminating S_2 will reduce the processing time from 32.722 [s] to 20.825 (= 32.722 - 11.897) [s] with minimal degradation in the accuracy of PCQA. Thus, eliminating S_2 would be a good option if reducing computation time is crucial.

Tables 2 and 4 show the calculation time required by S_5 was less than 0.01% of the total calculation time, while the PLCC and SROCC were improved by 0.4% and 0.2%, respectively. Thus, we included S_5 to improve PCQA accuracy in combination with the other scores with very limited added computation.

4.4. Experiment 3: Comparison with the conventional methods

Table 5 presents a comparative analysis of the proposed method against the conventional FR-PCQA methods with PLCC, SROCC, and average processing time across all the point clouds. The results demonstrate that the proposed method achieved the highest correlation coefficients across all the datasets. Moreover, the proposed method showed faster processing time compared with the accurate conventional methods such as point-to-plane (MSE) [18], PCQM [21], GraphSIM [22], and MSGraphSIM [23]. In Fig. 5, the performance of the proposed method and conventional methods is visually

Table 5: The correlation coefficients and processing time [s] of the proposed and conventional FR-PCQA methods with the three datasets. The **bold characters** show the best performance.

Method	BASICS (test set) [52]			ICIP20 [53]			WPC [54]		
	PLCC	SROCC	Time [s]	PLCC	SROCC	Time [s]	PLCC	SROCC	Time [s]
point-to-point (MSE) [17]	0.793	0.735	9.701	0.960	0.949	3.019	0.585	0.566	6.832
point-to-plane (MSE) [18]	0.848	0.799	49.122	0.963	0.956	11.506	0.489	0.481	32.847
angular similarity [46]	0.330	0.306	39.155	0.650	0.579	10.462	0.301	0.319	27.336
Y-MSE [17]	0.558	0.550	9.896	0.897	0.900	3.054	0.613	0.591	6.928
PointSSIM (geom) [19]	0.719	0.650	22.072	0.901	0.918	6.711	0.389	0.345	14.490
PointSSIM (color) [19]	0.652	0.620	23.682	0.941	0.913	7.088	0.492	0.471	15.281
PCQM [21]	0.829	0.739	256.463	0.952	0.960	82.801	0.570	0.550	214.197
GraphSIM [22]	0.849	0.773	613.652	0.943	0.931	207.532	0.701	0.691	382.798
MSGraphSIM [23]	0.841	0.773	645.589	0.951	0.945	220.107	0.727	0.724	348.183
Proposed (FRSVR)	0.914	0.878	32.722	0.975	0.965	10.075	0.819	0.803	20.608

Table 6: The correlation coefficients of the BASICS dataset (test set). An SVR model is trained with either the ICIP20 or BASICS training datasets. The former indicates a cross-dataset evaluation. The **bold characters** show the best performance.

Method	Training dataset	PLCC	SROCC
Proposed	ICIP20	0.900	0.861
Proposed	BASICS (training set)	0.914	0.878

depicted with a scatter plot. These findings highlight that the proposed method achieved a superior trade-off between accuracy and computation speed.

The proposed method showed comparatively lower correlation coefficients measured with the WPC dataset in contrast with the other datasets. Since the WPC dataset includes not only point clouds contaminated by compression errors but also those perturbed by various kinds of noise, such as downsampling and Gaussian noise, obtaining high correlation coefficients was challenging because noise has a wide variety of characteristics.

4.5. Experiment 4: Generalization capability of the proposed method

To assess the generalization capability of the proposed method, we conducted a cross-dataset evaluation. In this experiment, an SVR model was trained using all the point clouds in the ICIP20 dataset. After that, all the point clouds in the BASICS dataset (test set) were assessed by using the trained model. In Table 6, when we utilized the ICIP20 dataset for training an SVR model, a slight degradation occurred in correlation coefficients. However, the results were still sufficiently accurate compared with those of other conventional methods introduced in Table 5. While the BASICS dataset includes point clouds compressed by a deep learning-based compression method [7], the ICIP20 dataset does not include them. Consequently, differences in characteristics of compression distortion between training and test data resulted in some degree of degradation in performance.

4.6. Experiment 5: Effect of sampling strategy in the proposed method

As shown in Fig. 2, we introduce point cloud sampling to mitigate computation complexity in the proposed method.

Thus, we investigated the impact of the sampling on the performance. The graph construction parameters of the proposed method without sampling are the same as those of the proposed method with sampling. Table 7 shows that sampling strategy can significantly reduce the calculation time. For the BASICS and ICIP20 datasets, the impact on PLCC and SROCC was also very small. In contrast, the PLCC and SROCC of the WPC dataset decreased by sampling. Since the WPC dataset contains a variety of noises, such as Gaussian noise, unlike the other datasets, the sampling strategy may cause an adverse effect in capturing the noise characteristic. For example, although measuring Gaussian noise in color signals is easy in a dense point cloud, it may be difficult in a sparse point cloud because of the interference with color changes in the original signal. If a point cloud has a variety of noise and the accuracy is a critical issue, the sampling strategy may cause a bad effect.

5. Discussion of the limitation and further improvement

5.1. Accuracy

As shown in Table 5, there is room for improvement, especially regarding the accuracy of the WPC dataset. Since The proposed method integrates several FR-PCQA scores by SVR, it can be combined with other metrics. In this section, we introduce the combination with PCQM [21], which is a highly accurate conventional FR-PCQA method to show further improved accuracy. PCQM [21] uses eight types of FR scores called curvature comparison f_1 , curvature contrast f_2 , curvature structure f_3 , lightness comparison f_4 , lightness contrast f_5 , lightness structure f_6 , chroma comparison f_7 , and hue comparison f_8 . Here, we report the results when we utilize 13 types of FR-PCQA scores, including $f_1 \sim f_8$ and $S_1 \sim S_5$.

In this extra experiment, we verified all the subsets of 13 scores to train an SVR model. Thus, $2^{13} - 1 = 8191$ patterns were evaluated to determine the optimal configuration. Table 8 shows the top five subsets (selected scores) that were evaluated based on the average SROCC of the three datasets. When we utilized eight scores composed of $S_2, S_3, S_4, S_5, f_1, f_3, f_4,$ and f_5 , we achieved the best average SROCC (0.918). In particular, significant accuracy improvements were obtained for the WPC dataset with the scores derived from PCQM. This result shows

Table 7: The correlation coefficients and processing time of the proposed method with or without sampling. "Proposed (w/o sampling)" shows the results when point clouds without sampling are utilized for the proposed method.

Method	BASICS (test set) [52]			ICIP20 [53]			WPC [54]		
	PLCC	SROCC	Time [s]	PLCC	SROCC	Time [s]	PLCC	SROCC	Time [s]
Proposed (w/o sampling)	0.902	0.873	65.039	0.974	0.970	18.765	0.828	0.818	42.758
Proposed	0.914	0.878	32.722	0.975	0.965	10.075	0.819	0.803	20.608

Table 8: The correlation coefficients of the proposed method with the additional scores derived from PCQM [21]. "Ave SROCC" means the average of SROCCs of three datasets. The top five selected scores are listed based on the average SROCC in this table. The **bold characters** show the best performance.

Method	Selected scores	BASICS (test set)		ICIP20		WPC		Ave SROCC
		PLCC	SROCC	PLCC	SROCC	PLCC	SROCC	
Proposed + PCQM	$S_2, S_3, S_4, S_5, f_1, f_3, f_4, f_5$	0.907	0.886	0.975	0.970	0.899	0.898	0.918
Proposed + PCQM	$S_2, S_3, S_4, S_5, f_1, f_2, f_3, f_4, f_5$	0.897	0.882	0.976	0.973	0.900	0.899	0.918
Proposed + PCQM	$S_2, S_3, S_4, S_5, f_2, f_3, f_4, f_5$	0.897	0.883	0.978	0.972	0.899	0.896	0.917
Proposed + PCQM	$S_1, S_2, S_3, S_4, S_5, f_1, f_3, f_4, f_5$	0.897	0.875	0.979	0.974	0.900	0.899	0.916
Proposed + PCQM	$S_1, S_2, S_3, S_4, S_5, f_1, f_2, f_3, f_4, f_5$	0.888	0.874	0.978	0.974	0.900	0.899	0.915
Proposed	S_1, S_2, S_3, S_4, S_5	0.914	0.878	0.975	0.965	0.819	0.803	0.882

the potential for further improvement of the proposed method. However, PCQM has the problem of large computation time as shown in Table 5. In the future, we will improve the accuracy of the proposed method by considering new features that can be calculated more efficiently.

In addition, the results shown in Table 8 support the inclusion of S_5 because all of these top five subsets include S_5 . For example, S_1 was not adopted in the most accurate subset because S_2 shows similar assessment results to S_1 . On the other hand, the S_5 score, which takes into account the difference in the number of points, can capture degradation that the other scores do not consider.

5.2. Processing time

As shown in Table 5, while the proposed method performed faster than some of the conventional methods, the proposed method was not the fastest among all the conventional methods. Thus, further acceleration is one of our future challenges for achieving more efficient PCQA. Table 4 indicates that the computation time for graph construction is relatively large compared with other parts. Thus, fast computation for the graph construction part is necessary. To solve this problem, conventional fast KNN methods based on GPU implementation have been introduced [57, 58, 59]. As an alternative approach, an approximation-based fast graph construction method that performs real-time processing on over 1 million points has been proposed [60]. While this method [60] is faster than fast KNN methods [57, 58, 59], an inaccurate graph may be constructed and affect the accuracy of PCQA. In the future, we plan to assess these techniques to mitigate graph construction time and achieve faster PCQA.

6. Conclusion

In this paper, we proposed an accurate and fast FR-PCQA using SVR. Since the proposed method integrates multiple simple metrics effectively based on SVR, it performs a great trade-off between quality assessment accuracy and computation speed.

Our method was proposed for the ICIP 2023 PCVQA Grand Challenge, which only focuses on quality assessments of compression distortion. Therefore, there are still challenges in accurate assessments for the various kinds of noise (e.g., gaussian noise, down-sampling) other than compression distortion. While the incorporation of additional features, as discussed in Section 5.1, contributes to the improvement of accuracy, the computation time becomes significantly large. In the future, we aim to introduce new features that are suitable for such noise and efficiently calculated to improve the proposed method.

CRedit authorship contribution statement

Ryosuke Watanabe: Conceptualization, Methodology, Validation, Visualization, Formal analysis, Investigation, Software, Data curation, Writing - original draft, Writing - review & editing. **Shashank N. Sridhara:** Methodology, Investigation, Writing - review & editing. **Haoran Hong:** Methodology, Investigation, Writing - review & editing. **Eduardo Pavez:** Methodology, Investigation, Writing - review & editing. **Keisuke Nonaka:** Writing - review & editing, Funding acquisition. **Tatsuya Kobayashi:** Writing - review & editing, Funding acquisition. **Antonio Ortega:** Methodology, Investigation, Writing - review & editing, Supervision, Project administration.

Declaration of Competing Interest

The authors declare that they have no known competing financial interests or personal relationships that could have appeared to influence the work reported in this paper. There are no conflicts of interest regarding the publication of this study.

Funding

This work was supported by Ministry of Internal Affairs and Communications (MIC) of Japan (Grant no. JPJ000595).

References

- [1] Kevin Yu, Gleb Gorbachev, Ulrich Eck, Frieder Pankratz, Nassir Navab, and Daniel Roth. Avatars for teleconsultation: Effects of avatar embodiment techniques on user perception in 3D asymmetric telepresence. *IEEE Transactions on Visualization and Computer Graphics*, 27(11):4129–4139, 2021.
- [2] Priya M V and Dhanya S Pankaj. 3DYOLO: Real-time 3D object detection in 3D point clouds for autonomous driving. In *2021 IEEE International India Geoscience and Remote Sensing Symposium (InGARSS)*, pages 41–44, 2021.
- [3] Nova Eka Budiyanta, Eko Mulyanto Yuniarno, Tsuyoshi Usagawa, and Mauridhi Hery Purnomo. Normal vector direction-based 3D LiDAR point cloud planar surface removal for object cluster minimization in human activity monitoring system. In *2023 IEEE International Instrumentation and Measurement Technology Conference (I2MTC)*, pages 1–6, 2023.
- [4] Mostafa Agour and Thomas Kreis. Experimental investigation of holographic 3D-TV approach. In *2009 3DTV Conference: The True Vision - Capture, Transmission and Display of 3D Video*, pages 1–4, 2009.
- [5] Danillo B. Graziosi, Ohji Nakagami, Satoru Kuma, Alexandre Zaghetto, Teruhiko Suzuki, and Ali Tabatabai. An overview of ongoing point cloud compression standardization activities: video-based (V-PCC) and geometry-based (G-PCC). *APSIPA Transactions on Signal and Information Processing*, 9:e13, 2020.
- [6] Maurice Quach, Giuseppe Valenzise, and Frederic Dufaux. Learning convolutional transforms for lossy point cloud geometry compression. In *2019 IEEE International Conference on Image Processing (ICIP)*, pages 4320–4324, 2019.
- [7] Maurice Quach, Giuseppe Valenzise, and Frederic Dufaux. Improved deep point cloud geometry compression. In *2020 IEEE 22nd International Workshop on Multimedia Signal Processing (MMSP)*, pages 1–6, 2020.
- [8] Wenming Huang, Yuanwang Li, Peizhi Wen, and Xiaojun Wu. Algorithm for 3d point cloud denoising. In *2009 Third International Conference on Genetic and Evolutionary Computing*, pages 574–577, 2009.
- [9] Yiyao Zhou, Rui Chen, Yiqiang Zhao, Xiding Ai, and Guoqing Zhou. Point cloud denoising using non-local collaborative projections. *Pattern Recognition*, 120:108128, 2021.
- [10] Anique Akhtar, Zhu Li, Geert Van der Auwera, Li Li, and Jianle Chen. Pu-dense: Sparse tensor-based point cloud geometry upsampling. *IEEE Transactions on Image Processing*, 31:4133–4148, 2022.
- [11] Kaisiyuan Wang, Lu Sheng, Shuhang Gu, and Dong Xu. Sequential point cloud upsampling by exploiting multi-scale temporal dependency. *IEEE Transactions on Circuits and Systems for Video Technology*, 31(12):4686–4696, 2021.
- [12] Zeqing Fu and Wei Hu. Dynamic point cloud inpainting via spatial-temporal graph learning. *IEEE Transactions on Multimedia*, 23:3022–3034, 2021.
- [13] Ju He, Zeqing Fu, Wei Hu, and Zongming Guo. Point cloud attribute inpainting in graph spectral domain. In *2019 IEEE International Conference on Image Processing (ICIP)*, pages 4385–4389, 2019.
- [14] Tsung-Jung Liu, Yu-Chieh Lin, Weisi Lin, and C.-C. Jay Kuo. Visual quality assessment: recent developments, coding applications and future trends. *APSIPA Transactions on Signal and Information Processing*, 2:e4, 2013.
- [15] Zhou Wang, Alan C. Bovik, Hamid R. Sheikh, and Eero P. Simoncelli. Image quality assessment: from error visibility to structural similarity. *IEEE Transactions on Image Processing*, 13(4):600–612, 2004.
- [16] Zhou Wang, Eero P. Simoncelli, and Alan C. Bovik. Multiscale structural similarity for image quality assessment. In *The 37th Asilomar Conference on Signals, Systems and Computers, 2003*, volume 2, pages 1398–1402, 2003.
- [17] Rafael Mekuria, Zhu Li, Christian Tulvan, and Phil Chou. Evaluation criteria for PCC (point cloud compression). In *ISO/IEC JTC 1/SC29/WG11 Doc.*, number N16332, 2016.
- [18] Dong Tian, Hideaki Ochimizu, Chen Feng, Robert Cohen, and Anthony Vetro. Geometric distortion metrics for point cloud compression. In *2017 IEEE International Conference on Image Processing (ICIP)*, pages 3460–3464, 2017.
- [19] Evangelos Alexiou and Touradj Ebrahimi. Towards a point cloud structural similarity metric. In *2020 IEEE International Conference on Multimedia Expo Workshops (ICMEW)*, pages 1–6, 2020.
- [20] Davi Lazzarotto and Touradj Ebrahimi. Towards a multiscale point cloud structural similarity metric. In *25th International Workshop On Multimedia Signal Processing (MMSP)*, 2023.
- [21] Gabriel Meynet, Yana Nehmé, Julie Digne, and Guillaume Lavoué. PCQM: A full-reference quality metric for colored 3D point clouds. In *2020 Twelfth International Conference on Quality of Multimedia Experience (QoMEX)*, pages 1–6, 2020.
- [22] Qi Yang, Zhan Ma, Yiling Xu, Zhu Li, and Jun Sun. Inferring point cloud quality via graph similarity. *IEEE Transactions on Pattern Analysis and Machine Intelligence*, 44(6):3015–3029, 2022.
- [23] Yujie Zhang, Qi Yang, and Yiling Xu. MS-GraphSIM: Inferring point cloud quality via multiscale graph similarity. In *29th ACM International Conference on Multimedia*, page 1230–1238, 2021.
- [24] Marouane Tliba, Aladine Chetouani, Giuseppe Valenzise, and Frederic Dufaux. Point cloud quality assessment using cross-correlation of deep features. In *Proceedings of the 2nd Workshop on Quality of Experience in Visual Multimedia Applications, QoEVM '22*, page 63–68, 2022.
- [25] Xuemei Zhou, Evangelos Alexiou, Irene Viola, and Pablo Cesar. Point-PCA+: Extending PointPCA objective quality assessment metric. In *2023 IEEE International Conference on Image Processing Challenges and Workshops (ICIPCW)*, pages 1–5, 2023.
- [26] Aladine Chetouani, Giuseppe Valenzise, Ali Ak, Emin Zerman, Maurice Quach, Marouane Tliba, Mohamed Amine Kerkouri, and Patrick Le Callet. ICIP 2023 - point cloud visual quality assessment grand challenge, 2023. <https://sites.google.com/view/icip2023-pcvqa-grand-challenge/>.
- [27] Ryosuke Watanabe, Shashank N. Sridhara, Haoran Hong, Eduardo Pavez, and Antonio Ortega. ICIP 2023 challenge: Full-reference and non-reference point cloud quality assessment methods with support vector regression. In *2023 IEEE International Conference on Image Processing Challenges and Workshops (ICIPCW)*, pages 3654–3658, 2023.
- [28] Salima Bourbia, Ayoub Karine, Aladine Chetouani, Mohammed El Hassouni, and Maher Jridi. No-reference 3D point cloud quality assessment using multi-view projection and deep convolutional neural network. *IEEE Access*, 11:26759–26772, 2023.
- [29] Yu Fan, Zicheng Zhang, Wei Sun, Xiongkuo Min, Ning Liu, Quan Zhou, Jun He, Qiyuan Wang, and Guangtao Zhai. A no-reference quality assessment metric for point cloud based on captured video sequences. In *2022 IEEE 24th International Workshop on Multimedia Signal Processing*, pages 1–5, 2022.
- [30] Qi Liu, Hui Yuan, Honglei Su, Hao Liu, Yu Wang, Huan Yang, and Junhui Hou. PQA-Net: Deep no reference point cloud quality assessment via multi-view projection. *IEEE Transactions on Circuits and Systems for Video Technology*, 31(12):4645–4660, 2021.
- [31] Xinyu Wang, Ruijun Liu, and Xiaochuan Wang. No-reference point cloud quality assessment via contextual point-wise deep learning network. In *Cognitive Systems and Information Processing*, 2024.
- [32] Jian Xiong, Sifan Wu, Wang Luo, Jinli Suo, and Hao Gao. ψ -net: Point structural information network for no-reference point cloud quality assessment. In *2023 IEEE International Conference on Acoustics, Speech and Signal Processing*, pages 1–5, 2023.
- [33] Yipeng Liu, Qi Yang, Yiling Xu, and Le Yang. Point cloud quality assessment: Dataset construction and learning-based no-reference metric. *ACM Trans. Multimedia Comput. Commun. Appl.*, 19(2s), 2023.
- [34] Ziyu Shan, Qi Yang, Rui Ye, Yujie Zhang, Yiling Xu, Xiaozhong Xu, and Shan Liu. GPA-Net: No-reference point cloud quality assessment with multi-task graph convolutional network. *IEEE Transactions on Visualization and Computer Graphics*, pages 1–13, 2023.
- [35] Marouane Tliba, Aladine Chetouani, Giuseppe Valenzise, and Frédéric Dufaux. Pcca-graphpoint: Efficient deep-based graph metric for point cloud quality assessment. In *2023 IEEE International Conference on Acoustics, Speech and Signal Processing*, pages 1–5, 2023.
- [36] Gwennan Smitskamp, Irene Viola, and Pablo Cesar. Evaluation of point cloud features for no-reference visual quality assessment. In *2023 15th International Conference on Quality of Multimedia Experience*, pages 147–152, 2023.
- [37] Zicheng Zhang, Wei Sun, Xiongkuo Min, Tao Wang, Wei Lu, and Guangtao Zhai. No-reference quality assessment for 3D colored point cloud and mesh models. *IEEE Transactions on Circuits and Systems for Video Technology*, 32(11):7618–7631, 2022.
- [38] Irene Viola and Pablo Cesar. A reduced reference metric for visual qual-

- ity evaluation of point cloud contents. *IEEE Signal Processing Letters*, 27:1660–1664, 2020.
- [39] Qi Liu, Hui Yuan, Raouf Hamzaoui, Honglei Su, Junhui Hou, and Huan Yang. Reduced reference perceptual quality model with application to rate control for video-based point cloud compression. *IEEE Transactions on Image Processing*, 30:6623–6636, 2021.
- [40] Wei Zhou, Guanghui Yue, Ruizeng Zhang, Yipeng Qin, and Hantao Liu. Reduced-reference quality assessment of point clouds via content-oriented saliency projection. *IEEE Signal Processing Letters*, 30:354–358, 2023.
- [41] Evangelos Alexiou and Touradj Ebrahimi. Exploiting user interactivity in quality assessment of point cloud imaging. In *2019 Eleventh International Conference on Quality of Multimedia Experience (QoMEX)*, pages 1–6, 2019.
- [42] Hamid R. Sheikh and Alan C. Bovik. Image information and visual quality. *IEEE Transactions on Image Processing*, 15(2):430–444, 2006.
- [43] Qi Liu, Honglei Su, Zhengfang Duanmu, Wentao Liu, and Zhou Wang. Perceptual quality assessment of colored 3D point clouds. *IEEE Transactions on Visualization and Computer Graphics*, 29(8):3642–3655, 2023.
- [44] Zhou Wang and Qiang Li. Information content weighting for perceptual image quality assessment. *IEEE Transactions on Image Processing*, 20(5):1185–1198, 2011.
- [45] Zhouyan He, Gangyi Jiang, Zhidi Jiang, and Mei Yu. Towards a colored point cloud quality assessment method using colored texture and curvature projection. In *2021 IEEE International Conference on Image Processing (ICIP)*, pages 1444–1448, 2021.
- [46] Evangelos Alexiou and Touradj Ebrahimi. Point cloud quality assessment metric based on angular similarity. In *2018 IEEE International Conference on Multimedia and Expo (ICME)*, pages 1–6, 2018.
- [47] Mariette Awad and Rahul Khanna. Support vector regression. *Efficient Learning Machines: Theories, Concepts, and Applications for Engineers and System Designers*, pages 67–80, 2015.
- [48] Ingmar Lissner and Philipp Urban. Toward a unified color space for perception-based image processing. *IEEE Transactions on Image Processing*, 21(3):1153–1168, 2012.
- [49] Hugues Hoppe, Tony DeRose, Tom Duchamp, John McDonald, and Werner Stuetzle. Surface reconstruction from unorganized points. *SIG-GRAPH Comput. Graph.*, 26(2):71–78, 1992.
- [50] Chinthaka Dinesh, Gene Cheung, and Ivan V. Bajić. 3D point cloud color denoising using convex graph-signal smoothness priors. In *2019 IEEE 21st International Workshop on Multimedia Signal Processing (MMSp)*, pages 1–6, 2019.
- [51] John Platt. Sequential minimal optimization: A fast algorithm for training support vector machines. Technical Report MSR-TR-98-14, Microsoft, 1998.
- [52] Ali Ak, Emin Zerman, Maurice Quach, Aladine Chetouani, Aljosa Smolic, Giuseppe Valenzise, and Patrick Le Callet. BASICS: Broad quality assessment of static point clouds in a compression scenario. *IEEE Transactions on Multimedia*, 26:6730–6742, 2024.
- [53] Stuart Perry, Huy Phi Cong, Luís A. da Silva Cruz, João Prazeres, Manuela Pereira, Antonio Pinheiro, Emil Dumic, Evangelos Alexiou, and Touradj Ebrahimi. Quality evaluation of static point clouds encoded using MPEG codecs. In *2020 IEEE International Conference on Image Processing*, pages 3428–3432, 2020.
- [54] Honglei Su, Zhengfang Duanmu, Wentao Liu, Qi Liu, and Zhou Wang. Perceptual quality assessment of 3D point clouds. In *2019 IEEE International Conference on Image Processing (ICIP)*, pages 3182–3186, 2019.
- [55] ITU-R. Methodology for the subjective assessment of the quality of television pictures. ITU-R Recommendation, BT.500-14, 2019.
- [56] Ann Rohaly, Philip Coriveau, John Libert, Arthur Webster, Vittorio Baroncini, John Beerends, Jean-Louis Blin, Laura Contin, Takahiro Hamada, David Harrison, Jeffrey Lubin, Yukihiro Nishida, Ricardo Nishihara, John Pearson, Antonio Pessoa, Neil Pickford, Alexander Schertz, Massimo Visca, and Stefan Winkler. Video quality experts group: current results and future directions. volume 4067, pages 742–753, 2000.
- [57] Vincent Garcia, Eric Debreuve, and Michel Barlaud. Fast k nearest neighbor search using GPU. In *2008 IEEE Computer Society Conference on Computer Vision and Pattern Recognition Workshops*, pages 1–6, 2008.
- [58] J. Jakob and M. Guthe. Optimizing LBVH-construction and hierarchy-traversal to accelerate kNN queries on point clouds using the GPU. *Computer Graphics Forum*, 40(1):124–137, 2021.
- [59] Shengren Li and Nina Amenta. Brute-force k-nearest neighbors search on the GPU. In *Proceedings of the 8th International Conference on Similarity Search and Applications*, volume 9371, page 259–270, 2015.
- [60] Ryosuke Watanabe, Keisuke Nonaka, Eduardo Pavez, Tatsuya Kobayashi, and Antonio Ortega. Fast graph-based denoising for point cloud color information. In *ICASSP 2024 - 2024 IEEE International Conference on Acoustics, Speech and Signal Processing (ICASSP)*, pages 4025–4029, 2024.